PAPER

Check for updates

A reversible, colorimetric, pH-responsive indole-based hydrogel and its application in urea detection†

Yan Wang, Xuan Luo,* Longfei Zhang, Shuai Zhang [ID] and Lin Zhang [ID]*

A new type of pH-responsive indole-based (4-HINF) hydrogel, fabricated by a sol–gel method, was utilized as a platform for colorimetric detection of urea in aqueous solution. The colorimetric sensor was established by virtue of the synergistic effect of cation–π interaction and hydrogen bonding with good regenerative ability. The results exhibited linear response in the range of 0–10 mM with a limit of detection of 10 μM. The prepared 4-HINF hydrogel possessed high selectivity to pH change under complicated environments ensuring further applications in environmental and bio-systems.

1. Introduction

Urea, a metabolic product of animals and a fertilizer of plants, plays crucial roles in the development of chemistry and biochemistry. An abnormal urea level in blood and urine may cause many diseases, such as urinary tract obstruction, nephritic syndrome, and cachexia.[1–4] Additionally, the hydrolysis of urea will generate ammonium (NH_4^+) and bicarbonate ions (HCO_3^-), inducing a pH increase in the aqueous medium.[2,4] A slight pH fluctuation can largely affect the kinetics of a biochemical reaction.[5–7] For instance, abnormal pH values in humans are frequently in connection with metabolic disorders.[8] In agriculture, high urea concentration generally causes serious environmental and economic problems, such as soil alkalization and loss of nitrogen. Therefore, urea detection is significantly important in fields ranging from the food industry and environmental monitoring to clinical chemistry. Currently, a variety of sensors have been developed to detect urea, which are based on detecting pH change generated by the hydrolysis reaction of urea, including fluorescent sensors,[9–11] electrodes,[12,13] and colorimetric sensors.[3,14,15] Among these sensors, colorimetric probes have attracted increasing attention because they can be easily read by the naked eye and intuitively discriminated in a simple way.[14,15]

Recently, pH-sensitive hydrogels have been extensively investigated for their potential applications in detection and controlled release systems.[16–19] There is a considerable interest in developing responsive hydrogels using noncovalent bonding, such as hydrogen bonding, hydrophobic effect, and cation–π interactions.[20–23] Cation–π interaction, a noncovalent

interaction between an electron-rich π aromatic system (*e.g.*, phenylalanine, tyrosine, and tryptophan (Trp)) and a positively charged cation (*e.g.*, Na^+ and K^+), has received considerable attention, due to their vital roles in many research areas, including biology, organic synthesis, and molecular recognition.[22,23] Indole, the side-chain substituent of Trp, is a versatile reactive material for cation–π interaction. An increasingly large number of research groups are focusing on construction of indole-based responsive materials.[24,25] Previously, our research group has reported a series of smart materials by using indole as original materials.[26–29] To the best of our knowledge, there is no report in the literature on 4-hydroxyindole (4-HIN) based hydrogel with pH response.

In this work, we prepared 4-HINF hydrogel *via* sol–gel method (Fig. 1a). It was found that the optical and color properties of 4-HINF hydrogel responded to pH strongly due to the
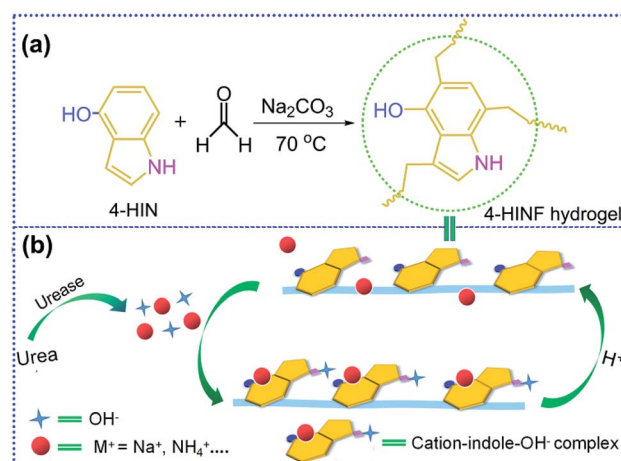
Research Center of Laser Fusion, China Academy of Engineering Physics, Mianyang, 621900, P. R. China. E-mail: zhlmy@sina.com

Fig. 1 (a) Fabrication of 4-HINF hydrogel. (b) The proposed mechanism of sensing for pH and urea by 4-HINF hydrogel.

host–guest interactions (cation–π interaction and hydrogen bonding). The adjustability of hydrogen bonding and cation–π interaction conferred the 4-HINF hydrogel remarkable recyclability (Fig. 1b). On the basis of this finding, a colorimetric sensor for urea in water system was developed.

2. Experimental

2.1 Materials and measurements

4-HIN was synthesized according to the reported method,[30] (the synthetic process and characterization were detailed in the ESI, Fig. S1–S3†). Formaldehyde aqueous (HCHO, 37%), sodium carbonate anhydrous (Na_2CO_3, AR), N-methylpyrrolidone (NMP, AR), hydrochloric acid (HCl, 12 M), potassium phosphate monobasic (KH_2PO_4, AR), sodium hydroxide (NaOH, AR), disodium phosphate dodecahydrate ($Na_2HPO_4 \cdot 12H_2O$, AR), urea (NH_2CONH_2, AR), urease ($Mr = 483\ 000$), sodium chloride (NaCl, AR), iron(III) chloride hexahydrate ($FeCl_3 \cdot 6H_2O$), calcium chloride anhydrous ($CaCl_2$, AR), potassium chloride (KCl, AR), ammonium sulfate (($NH_4)_2SO_4$, AR) and ascorbic acid (AA, AR) were used as received. Fourier-transform infrared (FT-IR) spectra were conducted on the Nicolet-5700 FT-IR spectrometer. ^1H NMR spectra were performed on Bruker AV-400 spectrometer at 400 MHz in DMSO-d_6 (δ 2.50 ppm). Solid-state ^{13}C NMR spectrum was conducted on a Bruker Avance III 400 NMR spectrometer. The scanning electron microscopy (SEM) images were made on an Ultra 55 microscope system. The transmission electron microscopy (TEM) image was obtained by using the TECNAI F20 system. The absorbance spectrum was measured on a SolidSpec-3700 spectrometer. X-ray photoelectron spectroscopy (XPS) was performed on the Escalab 250Xi system. X-ray diffraction (XRD) pattern was obtained with a X'Pert PRO X-ray diffractometer.

2.2 Preparation of 4-HINF hydrogel

4-HIN (0.532 g, 4 mmol) was dissolved in NMP (6 mL), deionized water (2 mL) and HCHO aqueous (650 μL) were mixed under vigorously stirred for 10 min. Then, Na_2CO_3 aqueous (4 mL, 10 mM) was added to the mixture and stirred for 20 min. The obtained solution (approximately 1.5 mL) was transferred into ampoule bottles (5.0 mL) and aged at 70 °C for 6 h. To remove any residue raw materials completely, 4-HINF hydrogel was washed with acetone and deionized water for 3 days, respectively. The final dried gel was obtained by freeze-dried for further testing.

2.3 Rheological properties

The dynamic rheological properties, including time dependence sweep, dynamic strain sweep, dynamic frequency sweep and dynamic temperature sweep of 4-HINF hydrogel were carried out with an ARES-G2 Rheometer using plate-and-plate a geometry (diameter 25 mm) with a proper gap. The shear storage or elastic modulus (G') as well as the shear loss or viscous modulus (G'') were measured.

2.4 Response to pH

Solutions with different pH values (7.0, 8.0, 9.0, 10.0, 11.0, 12.0 and 13.0) were used to investigate the pH-sensitivity of 4-HINF hydrogel. The ionic strength of various pH solutions was controlled to be 0.1 M by adjusting NaCl content. The pH values were adjusted by HCl (0.1 M) and NaOH (0.1 M) solution, and precisely determined using a pH-meter (pHS-3C$^+$). Then, the 4-HINF hydrogel (1.0 g) was added into the pH solutions (5.0 mL) for 5 min. The final 4-HINF hydrogel was freeze-dried overnight for optical testing.

2.5 Colorimetric detection of urea

Urease (100 μL, 15 U mL^{-1})and urea (100 μL) with different concentrations (0, 2, 5, 10, 20, 40, 50 and 100 mM) were added into PBS buffer solution (800 μL, 10 mM, pH = 7.40), and the solutions were incubated in a 37 °C bath for 30 min. Subsequently, 4-HINF hydrogels (1.0 g) were immersed into the above solutions which were further incubated for 5 min. Then, the optical spectrum was measured.

3. Results and discussion

3.1 Characterization of 4-HINF hydrogel

The FT-IR spectrum of 4-HINF hydrogel was shown in Fig. S4a.† The peak around 3405 cm^{-1} was assigned to the stretching vibration of phenolic hydroxyl and indole amine groups. The peak around 2923 cm^{-1} corresponded to the stretching vibration of methylene, the peaks at about 1626, 1432, 1382, 1239, and 1028 cm^{-1} were assigned to the vibrations of aromatic ring skeleton. In the solid-state ^{13}C NMR spectrum (Fig. S4b†), the peak at 131 ppm was ascribed to the central core phenyl carbon of phenyl ring carbons. The broad peaks at 146 and 126–112 ppm were ascribed to the indole group carbons. The characteristic absorption of the methylene carbons between two indole groups were observed at about 26 and 68 ppm. The XRD spectrum (Fig. S5†) revealed the 4-HINF hydrogel did not exhibit any crystalline pattern. Amorphous hydrogels were frequently obtained when synthesized by chemical crosslinking method.[31]

Fig. 2a–d illustrated the SEM images of 4-HINF hydrogel, it could be seen that a uniform network was formed by stacking
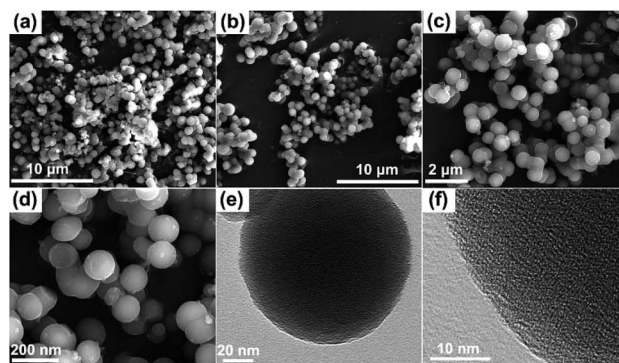

Fig. 2 (a–d) were the SEM images of 4-HINF hydrogel. (e) and (f) were the TEM images of 4-HINF hydrogel.

small volume spherical particles. The average size of the spherical particles was 60–100 nm. TEM images displayed the microstructure of 4-HINF hydrogel (Fig. 2e and f). The results confirmed the formation of cross-link between indole ring chains with formaldehyde.

3.2 Rheological properties of the 4-HINF hydrogel

The time-dependent rheological properties of 4-HINF hydrogel in the formation process were investigated at 70 °C (Fig. 3a). The strain amplitude (γ) and frequency (ω) were 1.0% and 6.28 rad s^{-1}, respectively. During short times, sols behaved as pure viscous liquids. With longer times, the mixture gelled, and a sudden increase in viscoelastic moduli (molecular weight gone to infinity) was observed at around 30 min. The G' and G'' confirmed the hydrogel-like behaviour,[32,33] and the hydrogel exhibited purple-red color (Fig. 4a). As time gone by, the curves of both moduli continue to increase until they reached a maximum value and stabilization after 6 h, revealing the complete formation of a polymeric structure. The values of G', G'', complex viscosity magnitude (η^*) and gelation time (t_g) were shown in Table S1.† Before the dynamic viscoelastic measurement, the linear viscoelastic region (LVR) was discussed by performing the γ from 0.01 to 100% at ω = 6.28 rad s^{-1} at T = 25 °C, as shown in Fig. 3b. In the LVE range (γ < 1.2%), the G' was greater than G'' for 4-HINF hydrogel, demonstrating that the total structural strength of hydrogel generally increased.[34] Frequency dependent at constant strain and temperature (γ = 1.0% and T = 25 °C) oscillatory shear rheology of the 4-HINF hydrogel (Fig. 3c) exhibited that the plateau-like G' was dominant over the G'' and no crossover point was observed, indicating a hydrogel-like behaviour.[34] To understand the behavior at different energy states, 4-HINF hydrogel was subjected to a temperature sweep study. Fig. 3d displayed the temperature dependence of G' and G'' for 4-HINF hydrogel under the
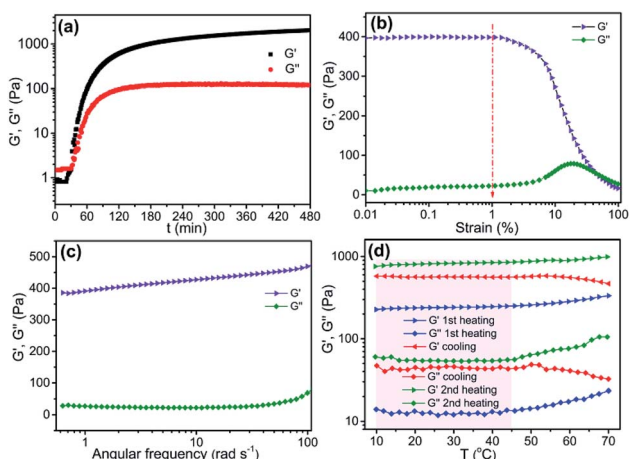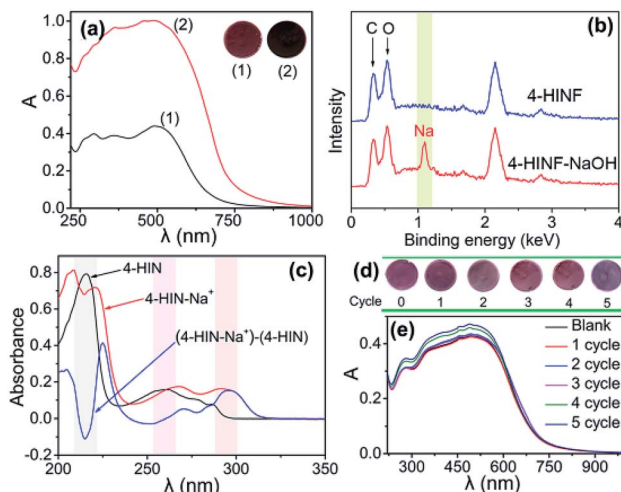

Fig. 4 (a) Optical spectra of 4-HINF hydrogel at different pH value. (1) pH = 7.0 and (2) pH = 13.0. The inset was the corresponding color change image. (b) XPS spectra of 4-HINF and 4-HINF–NaOH. (c) Absorption spectra of 4-HIN in the absence and presence of equi-molar amount of NaOH. The blue line displayed the corresponding difference spectrum for 4-HIN–Na$^+$. (d) Image and (e) optical spectra of 4-HINF hydrogel after different cycle.

heating–cooling–heating process (10–70–10–70 °C) at ω = 6.28 rad s^{-1} and γ = 1.0%. During the entire heating–cooling–heating circle, G' was throughout higher than G'', indicating the completion of gelation and an elastic hydrogel network. Starting from 10 to 45 °C in the first heating process, the moduli were roughly independent of temperature, and yet G' decreased very slightly with elevation of temperature, suggesting the stable cross-linking structure.[35] The moduli increased gradually with further increase of temperature from 45 to 70 °C, which might be caused by the formation of a denser network. In addition to the water evaporation factor, the increased physical cross-linking at elevated temperature also contributed to the positive dependence of moduli on the temperature ranging from 45 to 70 °C (known as thermal-induced hardening of hydrogels).[36]

3.3 Mechanism for pH and urea sensing

The sensing module that responded to pH and urea by 4-HINF hydrogel was illustrated in Fig. 1b. Indole, the side chains of the Trp, could participate non-covalent interactions both hydrogen bonding and cation–π interaction *via* indole amine and the π electric system, respectively. In this procedure, cation ions (*e.g.*, Na$^+$ and NH$_4^+$) oriented above the indole ring plane forming cation–indole complex, and the π electron density of indole shifted toward the cations,[37,38] leading to a charge deficit in the indole highest occupied molecular orbital (HOMO). Subsequently, the electron in HOMO-2 of indole transferred to the HOMO, and the radical character of cation–π interaction stemming from the electrostatic dislocation,[39–41] which resulted in a visible absorption at 500 nm (curve (1) in Fig. 4a). The pK_a for the indole aqueous solution (16.9) was higher than phenolic hydroxyl,[42] so indole amine was not ionized in the basic solution (pH range from 7.0 to 13.0). Therefore, the cation–indole–OH$^-$

Fig. 3 Dynamic viscoelastic performance (G' and G'') of 4-HINF hydrogel. (a) Time dependence at γ = 1.0%, ω = 6.28 rad s^{-1} and T = 70 °C. (b) Strain dependence at ω = 6.28 rad s^{-1} and T = 25 °C. (c) Frequency dependence at γ = 1.0% and T = 25 °C. (d) Temperature dependence during a heating–cooling–heating circle (10–70–10–70 °C) at γ = 1.0% and ω = 6.28 rad s^{-1}.

complex by the help of hydrogen bonding of indole amine would be formed. Moreover, the phenolic hydroxyl group could be deprotonated to from oxygen anion in the basic condition. It was reasonable to assume that the binding of deprotonated hydroxyl group to Na^+ was significant to the Na^+ to participate in the cation–π interaction. The bonding of Na^+ by negatively charged hydroxyl oxygen would partly decreased the oxidative reactivity of Na^+ against the π electron system, which could further stabilize cation–indole complex. Hence, more stable cation–indole–OH^- complex was formed with the help of hydrogen bonding between indole amine and OH^-. As pH increasing, the amount of Na^+ and OH^- increased, resulting in an increase in the absorbance intensity (curve (2) in Fig. 4a). Additionally, the color of 4-HINF hydrogel gradually changed from purple-red to black accompanied by pH value increased for the host–guest interactions (hydrogen bonding and cation–π interaction). Interestingly, the cation–π interaction and hydrogen bonding could be reversibly installed and removed by adjusting the pH from basic to acidic or neutral. The reason might be the competitive interaction of H^+ and the coordination effect of hydroxyl group, which would destroy the cation–π interaction.

The proposed colorimetric sensor for urea was based on detecting pH change generated by the enzymatic-catalyzed reaction (eqn (1)):

$$NH_2CONH_2 + 3H_2O \xrightarrow{\text{urease}} 2HN_4^+ + HCO_3^- + OH^- \quad (1)$$

The hydrolysis of urea yielded NH_4^+, HCO_3^- and OH^- in the presence of urease, leading to the increase in pH of solution. Indole, NH_4^+ and OH^- formed NH_4^+–indole–OH^- complex. Along with the increase of concentration of urea, the amount of NH_4^+ and OH^- increased, creating an increasing in the number and stability of NH_4^+–indole–OH^- complex. Consequently, the absorbance increased accompanied by a color altering.

The possibility of the 4-HIN–Na^+ interaction in the presence of OH^- was confirmed by XPS analysis (Fig. 4b). Consistent with their chemical structures, 4-HINF surface contained carbon (0.37 keV), oxygen (0.53 keV), while the 4-HIN–Na^+ surface contained carbon, oxygen and sodium (1.2 keV). The cation–π interaction of 4-HIN and Na^+ was further tested by UV-vis absorption spectrum, as shown in Fig. 4c. Comparing to the spectrum of 4-HIN and 4-HIN–Na^+, a negative and a positive absorption peaks were observed at 217 and 225 nm in the difference spectrum of 4-HIN–Na^+, respectively. The negative/positive absorption peak pair reflected the weakening and a slight red-shift of the strong B_b transition of the indole ring.[43,44] The similar absorption peak pair above 220/230 nm was also observed in reported previously other cation–π interaction (K^+ and Trp indole ring),[43] indicating that the 4-HIN–Na^+ interaction in the presence of OH^- was also could be categorized as cation–π interaction.

The pH response performance of 4-HINF hydrogel exhibited remarkable reversibility. As illustrated in Fig. 4e, the increase in absorbance of 4-HINF hydrogel produced by the pH ranging from 7.0 to 13.0 could be effectively restored *via* adding HCl to

revert the pH back from 13.0 to 7.0. Even after 5 cycles, the color and absorbance of 4-HINF hydrogel maintained a slight variation (Fig. 4d and e).

The optical spectrum of the 4-HINF hydrogel in aqueous solution with different pH values were investigated, as shown in Fig. 5. The color of 4-HINF hydrogel gradually changed from purple-red to black. Simultaneously, the system exhibited an enhancement in A at 500 nm as the pH increased with the linear relation $A = 0.1032\text{pH} - 0.2782$ ($R^2 = 0.991$). The linear detection range (7.0–13.0) made the 4-HINF hydrogel a promising responsive material for application pH detection in water and biological systems.

3.4 Urea sensing

Then, the application in detection of urea by 4-HINF hydrogel was explored, as shown Fig. 6a. The pH value of the solutions containing different concentration of urea gradually increased from 7.41 to 9.06. The color of 4-HINF hydrogel in corresponding solutions changed from purple to blue purple. The absorbance of the 4-HINF hydrogels at 500 nm gradually increased along with the incremental concentration of urea (Fig. 6b). The calibration curve for A against urea concentration was linear in the range from 0 to 10 mM and fitted the linear equation $A = 0.4871 + 0.00346 c_{\text{urea}}$ (c_{urea} represented the concentration of urea, $R^2 = 0.992$) (Fig. 6c). The concentration of urea in blood was about 2.5–7.5 mM.[45] Thus, the linear range of 0–10 mM for urea could fulfil the needs of practical determination. The limit of detection was 10 μM at a signal-to-noise ratio of 3 and the relative standard deviation (RSD) was 6.6%, making the proposed colorimetric sensor was a promising candidate for biosystem and environmental monitoring.

The selectivity of the proposed assay with different possible interfering substances was further investigated, as illustrated in Fig. 7. The relative absorbance ($\Delta A = A - A_0$, where A and A_0 are the absorbance of 4-HINF hydrogel in the absence and presence of different interferences at 500 nm, respectively.) was used to study the selectivity. As shown in Fig. 7c, the individual presence of each kind of some common ions including Na^+, K^+, NH_4^+, Ca^{2+} and Fe^{3+} had negligible influence on the urea detection. AA displayed slight interference for the detection of
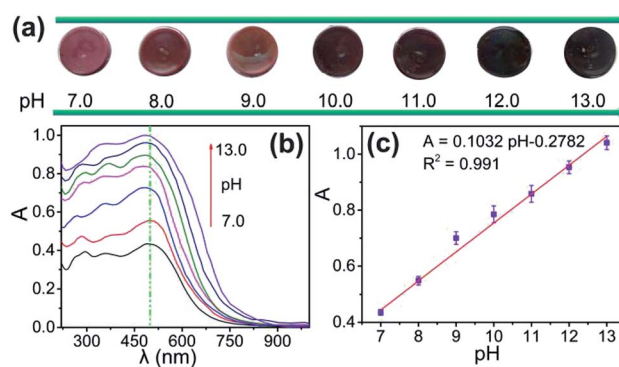

Fig. 5 (a) Image of color change and (b) optical spectra of 4-HINF hydrogels at different pH values. (c) The linear relationship between the A and calibration plots for pH values.
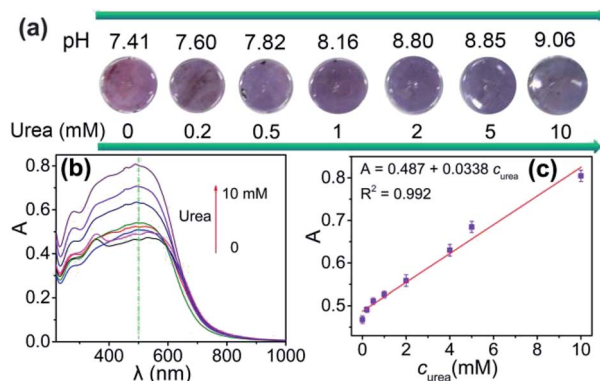
Fig. 6 (a) pH value and the color image and (b) optical spectra of 4-HINF hydrogels at different concentration of urea. (c) The linear relationship between the A and calibration plots for urea.
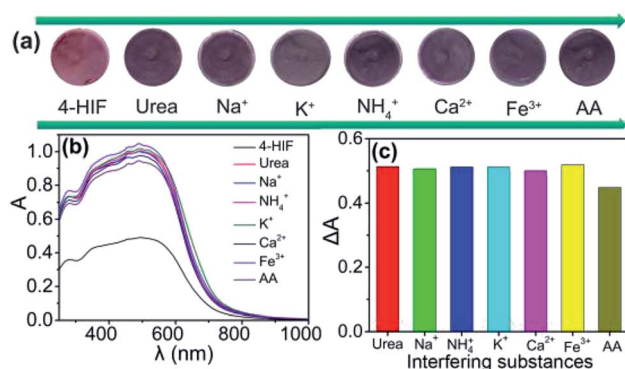

Fig. 7 (a) Image of color change; (b) optical spectra; (c) ΔA of 4-HINF hydrogels after immersed in urea solution in the presence of different interfering substances.

urea because AA would generate H^+ with the increase of pH value. The high selectivity may benefit from the hydrolysis mechanism of urea catalysed by urease, which resulted in a pH change of solution to give different optical and color response towards 4-HINF hydrogel.

4. Conclusions

In summary, we have constructed an indole-based pH-responsive hydrogel (4-HINF) *via* sol–gel method. Due to the synergistic effect of cation–π interaction and hydrogen bonding, the 4-HINF hydrogel exhibited an optical response to pH change with a satisfactory reversibility. Interestingly, the pH-responsive performance could be visual detected by making use of the color change for the host–guest interactions. On this basis, a colorimetric sensing platform for urea detection was developed. The linear detection ranged from 0 to 10 mM with the limit of detection of 10 μM. Moreover, 4-HINF hydrogel exhibited good selectivity in complicated surroundings. The good performance for pH and urea sensing suggested that 4-HINF hydrogel is expected to have great potential applications in bioassays and environmental monitoring.

Conflicts of interest

The authors declare that they have no conflict of interest.

Acknowledgements

References

1 G. P. Nikoleli, D. P. Nikoleli and C. Methenitis, *Anal. Chim. Acta*, 2010, **675**, 58.

2 S. M. U. Ali, Z. H. Ibupoto, S. Salman, O. Nur, M. Willander and B. Danielsson, *Sens. Actuators, B*, 2011, **160**, 637.

3 K. Wang, L. Yang, W. Wei, L. Zhang and G. Chang, *J. Membr. Sci.*, 2018, **549**, 23.

4 Y. Li, L. Yang, M. Du and G. Chang, *Analyst*, 2019, **144**, 1260.

5 Y. G. Wang, K. J. Zhou, G. Huang, C. Hensley, X. N. Huang, X. P. Ma, T. Zhao, B. D. Summer, R. J. DeBerardinis and J. M. Gao, *Nat. Mater.*, 2014, **13**, 204.

6 Y. Hu, H. Cheng, X. Zhao, J. Wu, F. Muhammad, S. Lin, J. He, L. Zhou, C. Zhang, Y. Deng, P. Wang, Z. Zhou, S. Nie and H. Wei, *ACS Nano*, 2017, **11**, 5558.

7 L. Yang, C. Wang, G. Chang and X. Ren, *Sens. Actuators, B*, 2017, **240**, 212.

8 L. L. Shi, Y. F. Liu, T. Wang, Y. Ding, Y. Cao, Z. Li and H. Wei, *Analyst*, 2018, **143**, 741.

9 R. Wang, C. W. Yu, F. Yu, L. X. Chen and C. Yu, *TrAC, Trends Anal. Chem.*, 2010, **29**, 1004.

10 W. Shi, X. Li and H. Ma, *Angew. Chem., Int. Ed.*, 2012, **124**, 6538.

11 L. L. Wu, X. L. Li, N. Q. Jia and N. Jia, *Anal. Chem.*, 2016, **88**, 8332.

12 M. Zhang, S. Karra and W. Gorski, *Anal. Chem.*, 2013, **85**, 6026.

13 S. Srivastava, M. A. Ali, P. R. Solanki, P. M. Chavhan, M. K. Pandey, A. Mulchandani, A. Srivastavab and B. D. Malhotra, *RSC Adv.*, 2013, **3**, 228.

14 H. H. Deng, G. L. Hong, F. L. Lin, A. L. Liu, X. H. Xia and W. Chen, *Anal. Chim. Acta*, 2016, **915**, 74.

15 H. H. Deng, G. W. Wu, Z. Q. Zou, H. P. Peng, A. L. Liu, X. H. Lin, X. H. Xia and W. Chen, *Chem. Commun.*, 2015, **51**, 7847.

16 M. M. Zhao, P. L. Wang, Y. J. Guo, L. X. Wang, F. Luo, B. Qiu, L. H. Guo, X. Su, Z. Y. Lin and G. N. Chen, *Talanta*, 2018, **176**, 34.

17 Y. Zhao, C. Shi, X. Yang, B. Shen, Y. Sun, Y. Chen, X. Xu, H. Chen, K. Yu, B. Yang and Q. Lin, *ACS Nano*, 2016, **10**, 5856.

18 M. M. C. Bastings, S. Koudstaal, R. E. Kieltyka, Y. Nakano, A. C. H. Pape, D. A. M. Feyen, F. Slochteren, P. A. Doevendans, J. P. G. Sluijter, E. W. M. Steven, A. J. Chamuleau and P. Y. W. Dankers, *Adv. Healthcare Mater.*, 2014, **3**, 70.

19 G. Tkalec, Ž. Knez and Z. Novak, *Microporous Mesoporous Mater.*, 2016, **224**, 190.

20 K. Wang, L. Yang, W. Wei, L. Zhang and G. Chang, *J. Membr. Sci.*, 2018, **549**, 23.

21 G. Chang, Y. Wang, C. Wang, Y. Li, Y. Xu and L. Yang, *Chem. Commun.*, 2018, **54**, 9785.

22 W. Wei, G. Chang, Y. Xu and L. Yang, *J. Mater. Chem. A*, 2018, **6**, 18794.

23 P. Yang, L. Yang, Y. Wang, L. Song, J. Yang and G. Chang, *J. Mater. Chem. A*, 2019, **7**, 531.

24 G. Chitra, D. S. Franklin, S. Sudarsan, M. Sakthivel and S. Guhanathan, *Int. J. Biol. Macromol.*, 2017, **95**, 363.

25 P. Yang, L. Yang, J. Yang, X. Luo and G. Chang, *High Perform. Polym.*, 2019, **31**, 238.

26 G. Chang, L. Yang, J. Yang, M. P. Stoykovich, X. Deng, J. Cui and D. Wang, *Adv. Mater.*, 2018, **30**, 1704234.

27 G. Chang, L. Yang, S. Liu, R. Lin and J. You, *Polym. Chem.*, 2015, **6**, 697.

28 G. Chang, Z. Shang, T. Yu and L. Yang, *J. Mater. Chem. A*, 2016, **4**, 2517.

29 L. Yang, G. Chang and D. Wang, *ACS Appl. Mater. Interfaces*, 2017, **9**, 15213.

30 X. Guo, Z. Peng, S. Jiang and J. Shen, *Synth. Commun.*, 2011, **41**, 2044.

31 C. Spagnol, F. H. A. Rodrigues, A. G. B. Pereira, A. R. Fajardo, A. F. Rubira and E. C. Muniz, *Cellulose*, 2012, **19**, 1225.

32 Z. Zapata-Benabithe, F. Carrasco-Marín, J. de Vicente and C. Moreno-Castilla, *Langmuir*, 2013, **29**, 6166.

33 Z. Zapata-Benabithe, J. de Vicente, F. Carrasco-Marín and C. Moreno-Castilla, *Carbon*, 2013, **53**, 402.

34 R. Xing, K. Liu, T. Jiao, N. Zhang, K. Ma, R. Zhang, Q. Zou, G. Ma and X. Yan, *Adv. Mater.*, 2016, **28**, 3669.

35 J. Han, T. Lei and Q. Wu, *Carbohydr. Polym.*, 2014, **102**, 306.

36 S. A. Oleyaei, S. M. A. Razavi and K. S. Mikkonen, *Carbohydr. Polym.*, 2018, **192**, 282.

37 L. J. Juszczak and A. S. Eisenberg, *J. Am. Chem. Soc.*, 2017, **139**, 8302.

38 W. L. Zhu, X. J. Tan, C. M. Puah, J. D. Gu, H. L. Jiang, K. X. Chen, C. E. Felder, I. Silman and J. L. Sussman, *J. Phys. Chem. A*, 2000, **104**, 9573.

39 M. Aschi, F. Mazza and A. Nola Di, *J. Mol. Struct.: THEOCHEM*, 2002, **587**, 177.

40 T. T. Goodnow, M. V. Reddington, J. F. Stoddart and A. E. Kaifer, *J. Am. Chem. Soc.*, 1991, **113**, 4335–4337.

41 A. Moretto, F. Formaggio, M. Crisma, B. Kaptein, Q. Broxterman and C. Toniolo, *J. Pept. Res.*, 2005, **65**, 15.

42 G. Yagil, *Tetrahedron*, 1967, **23**, 2855.

43 H. Yorita, K. Otomo, H. Hiramatsu, A. Toyama, T. Miura and H. Takeuchi, *J. Am. Chem. Soc.*, 2008, **130**, 15266.

44 A. Okada, T. Miura and H. Takeuchi, *Biochemistry*, 2001, **40**, 6053.

45 Y. Song, H. Liu, H. Tan, F. Xu, J. Jia, L. Zhang, Z. Li and L. Wang, *Anal. Chem.*, 2014, **86**, 1980.